

In situ Strain Monitoring in Gas Tungsten Arc Welding Processes*

Zongyao Chen, Jian Chen, Zhili Feng, Yuming Zhang, Senior Member, IEEE

Abstract—Strain/stress evolution during welding is essential to understand material's mechanical behavior and the formation of weld defects such as distortion, cracks and residual stresses. In-situ measurement of strain has been very challenging due to the impact from high temperature and intense arc light. In this work, a newly-developed integrated optical system was utilized to monitor material's thermal and strain field adjacent to the fusion line during GTAW process. It was found that the variation of the measurement data could be positively correlated to the change of welding parameters and the characteristics of the final weldment. The purpose of this work is to develop a real-time welding quality monitoring system to proactively prevent the formation of certain weld defects.

I. INTRODUCTION

Gas tungsten arc welding (GTAW) is widely used in industry where high quality of component integrity and safety is required. It is crucial to eliminate weld defects such as partial penetration, cracks, incomplete fusion. Since detecting and repairing the weld defect is always time-consuming and expensive, real time monitoring and controlling welding process is necessary to avoid the formulation of those defects. In previously research [1-3], defect such as lack of penetration and lack of fusion can be detected by measuring weld pool shape geometry in real time. Various sensing technique such as vision-based, thermal-based method has been investigated to control the bead width and penetration depth [4, 5].

Thermomechanical evolution during welding plays an important role in understanding material's mechanical behavior and the formation of weld defects such as distortion, cracks and residual stresses. The conventional contact strain measurement using strain gauge is not suitable for high temperature conditions. The non-contact techniques such as holographic measurement, electronic speckle pattern

interferometry require complicated optical system and they are sensitive to arc light [6-8].

Digital image correlation (DIC) technique is a non-contact method that can measure the full-field displacement and strain on the material surface. It is relatively simple to setup for in-situ measurement. Although strain measurement using DIC has been studied [9-16] and attempted in some welding applications for several years [16-19], in-situ DIC measurement during welding is still very challenging. First, the intense welding arc light affects the quality of the images obtained from camera sensor. Second, the speckle pattern on the surface is vulnerable to the high temperature. When the measurement gets close to the welding torch, the thermal and electromagnetic radiation imposes significant influence on the optical system. Previous studies have used DIC to measure the strain on the workpiece during arc welding [20, 21]. However, most of these experimental measurements were conducted far away from the fusion zone, or at the back side of the workpiece. Recently, a new high-temperature DIC has been successfully developed to measure the strain field adjacent to the weld pool[7].

Thermal history in materials during welding is another critical factor affecting the quality of the weldment. Previous studies suggested non-uniform thermal expansion and liquid metal shrinkage near the weld pool result in weld distortion and residual stresses[21, 22]. Thermal analysis of welding process has been conducted by many researchers [7]. The infrared camera (IR) has been widely used to acquire the full temperature field. However, the IR camera only measures infrared intensity. Converting the IR intensity to real temperature remains challenging due to the uncertainty of emissivity[23, 24].

In this paper, an integrated multi-sensor experiment setup was established to measure the full field strain and temperature change during arc welding. The strain was monitored using the newly-developed high-temperature DIC system [7]. The thermal field was measured by an IR camera with the assistance of thermocouples for emissivity calibration. The preliminary data show that, by varying welding current and speed, the measured strain and temperature fields, as well as the shape and size of the resultant weld bead, changed correspondingly.

II. EXPERIMENTAL METHOD

A. Experimental setup

The integrated experiment system for strain measurement is shown in Fig.1. A camera was used to take the images of speckle pattern for DIC strain measurement. A number of special treatments were used to enhance the DIC image quality during welding. The 304 stainless steel specimen (200mm long, 100mm wide and 6mm thick) was clamped firmly on a strong backing plate. The distance between camera and the

*This manuscript has been authored by UT-Battelle, LLC under Contract No. DE-AC05-00OR22725 with the U.S. Department of Energy. The United States Government retains and the publisher, by accepting the article for publication, acknowledges that the United States Government retains a non-exclusive, paid-up, irrevocable, world-wide license to publish or reproduce the published form of this manuscript, or allow others to do so, for United States Government purposes. The Department of Energy will provide public access to these results of federally sponsored research in accordance with the DOE Public Access Plan (<http://energy.gov/downloads/doe-public-access-plan>).

Zongyao Chen is with the Department of Mechanical, Aerospace, and Biomedical Engineering, University of Tennessee, Knoxville, TN 37996 USA (e-mail: zchen25@utk.edu).

Jian Chen is with the Oak Ridge National Laboratory (ORNL), TN 37831 USA. (phone: 865-576-5974; e-mail: chenj2@ornl.gov).

Zhili Feng is with the Oak Ridge National Laboratory (ORNL), TN 37831 USA. (e-mail: fengz@ornl.gov).

YuMing Zhang is with Institute for Sustainable Manufacturing and Department of Electrical Engineering, University of Kentucky, Lexington, KY 40506, USA (e-mail: yuming.zhang@uky.edu).

specimen surface was fixed at 15 cm. A special high-temperature speckle pattern that could survive up to the temperature of material's melting point was applied on the surface prior to welding for DIC measurement [7]. In order to calibrate surface emissivity to convert IR intensity to actual temperature, two sets of thermocouple were attached on the surface for temperature measurement at the pre-determined locations.

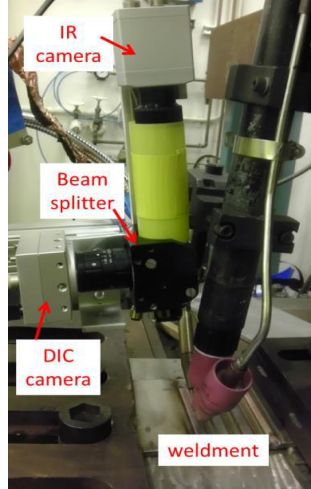


Figure 1. Experiment setup for in-situ strain measurement

As shown in Fig.1, bead on plate GTAW experiment was conducted on the weld specimen with the plate in horizontal position. A 0.045 diameter ER308L filler wire was fed to the weld pool at 20 inch/min. The arc voltage was set at 12V. Argon shielding gas at 10 CFH flow rate was also applied to protect the surface from oxidation. Four welding trials with different welding currents and welding speeds were conducted with the welding parameters listed in Table 1. To further investigate the influence of welding defect, the position of the weld feeder was changed to generate welding defect in experiment set IV.

Table 1. Welding process parameters.

Data set	Current (A)	Travel speed (inch/min)	Voltage(V)
I	160	7	12
II	160	10	12
III	130	10	12
IV	130	7	12

B. Strain Measurement using Digital Image Correlation

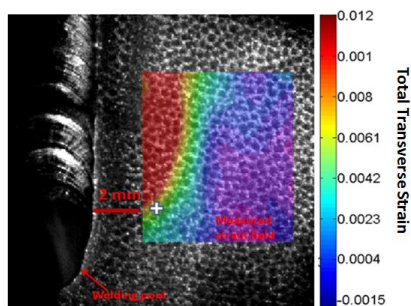


Figure 2. In-situ strain measurement using DIC

The DIC images were taken using the special optical and filtering system [7]. As shown in Fig. 2, the interference from the welding arc was effectively suppressed. The liquid weld pool and weld bead could be partially observed. A 2mm-wide oxidation band was observed which affected the strain measurement by DIC. Thus, this region was excluded for the strain measurement. Strain calculation was conducted using VIC-2D software from Correlated Solution.

Normally the accuracy of strain measurement by DIC algorithm is on the order of $100\mu\text{m}/\text{m}$ [9]. However, in most welding applications, noise level as high as $1000\mu\text{m}/\text{m}$ can be expected due to the arc light and high temperature[20]. This noise can be explained by the air turbulence near the hot weld pool surface causing shimmering and distortion of some of the DIC images. Thus, to reduce the noise, the strain data calculated by DIC was smoothed via Savitzky-Golay filter pixel by pixel throughout the entire region of interest (ROI).

C. Temperature Field Measurement

The collimated IR image frame synchronized to the DIC image frame (Fig. 2) is shown in Fig. 3. The IR intensity data in the same ROI as in Fig. 2 was extracted for further temperature calibration analysis. It is noted that the extracted IR intensity at each selected location was an average data within a set of neighboring pixels (corresponding to a region of approximately $\phi 0.5\text{mm}$) in the IR images. Then, the extracted IR data adjacent to the thermocouples were compared to the thermocouple measurement. The comparison is plotted in Fig. 4. The measured data was fitted to a polynomial curve with least square estimation to implicitly represent the surface emissivity (IR intensity vs. temperature relation). It was also found that the surface condition within the ROI had negligible change after welding. Therefore, the fitting curve in Fig. 4 was further used to calculate the actual temperature throughout the ROI.

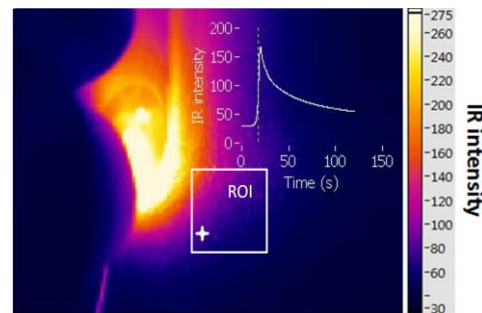


Figure 3. Real time temperature field monitoring using infrared camera (IR)

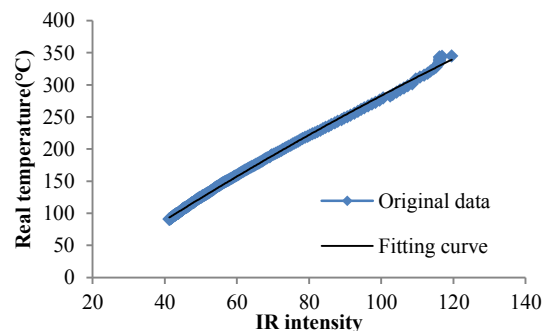


Figure 4. Calibration curve between IR intensity and real temperature

III. EXPERIMENT RESULT AND DISCUSSION

Fig.5 shows the top view of the first three welds performed at different parameters given in Table 1. The cross-section view in Fig. 6 shows the bead size after etching. Weld I had the largest fusion zone due to its high current and slow travel speed (consequently, high heat energy input calculated by equation 3) comparing to that of Welds II and III.

$$H_{net} = \frac{EI f_1}{v} \quad (3)$$

The E is the voltage, I is the welding current, v is the travel speed, f_1 is the heat transfer efficiency.



Figure. 5 Top view of weld

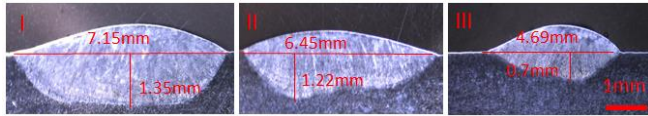


Figure.6 Cross-section of weld

As mentioned above, a data filtering method was applied to reduce the noise introduced by high temperature during welding. Fig.7 demonstrates the effectiveness of such filtering method. The raw DIC strain data has a noise level as high as 1000 $\mu\text{m}/\text{m}$.

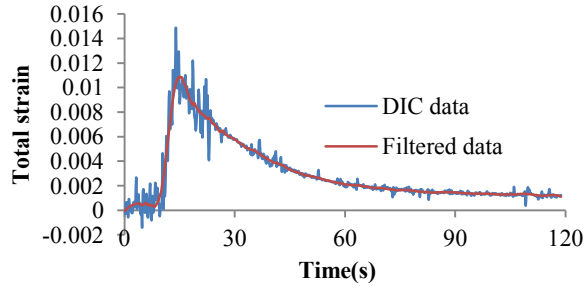


Figure 7. DIC strain data filtering

For all welds (I-III) in Table 1, the strain field in essentially the same location ($8 \times 10 \text{ mm}$) was calculated. As shown in Fig. 8, the strain field maps of three different welds are shown in the image frame when the liquid weld pool has just moved away from the ROI. Comparing the strain field between the three welds, the strain inside this area was largely reduced by varying the current, which indicates change of welding current (from 160A to 130A) had more influence on resultant transverse strain distribution than that of welding speed (from 7in/min to 10in/min)

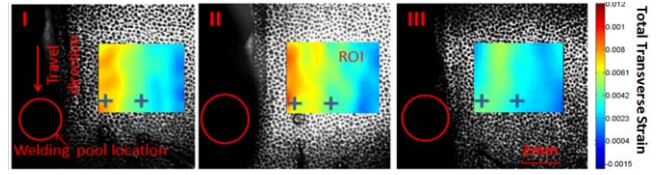


Figure. 8 Comparison of Full field strain calculation using DIC

Two points inside the ROI were selected (2.5mm and 5mm from the fusion boundary) for further discussion. The strain curves of all three welds are plotted in Fig.9. Overall, the transverse strain in both locations increased with the heat input. The strain at 2.5mm was higher than that at 5mm. The calibrated temperature history curves at the same two locations are also plotted in Fig.10.

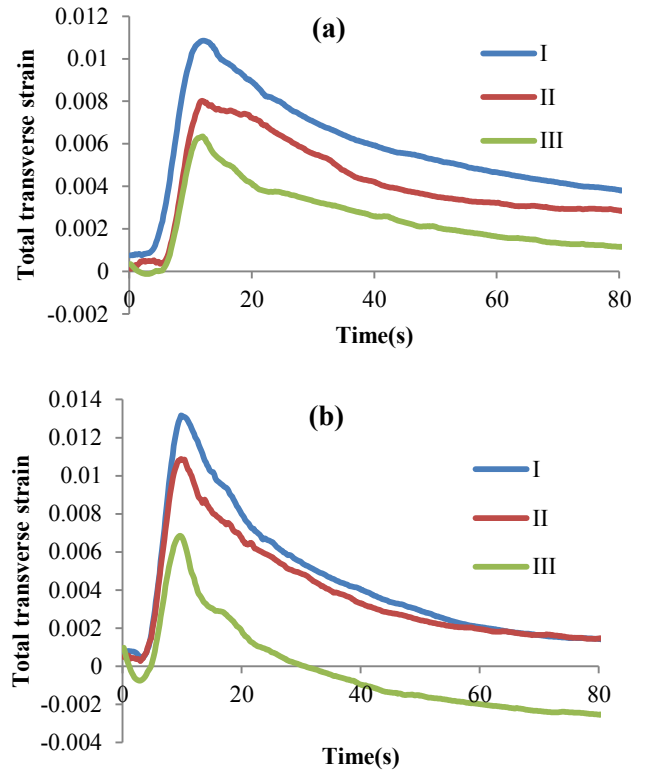


Figure. 9 (a)Total transverse strain comparison at 5 mm to the weld, (b)Total transverse strain comparison at 2.5 mm to the weld

Table 2 lists some of the feature of the experiment result. By comparing all the features, it is evident that changing the welding current had more effect on the strain rather than the temperature peak. On the other hand, reducing the welding travel speed increased the peak of temperature at same distance to the fusion boundary.

The preliminary results discussed above demonstrated the feasibility of utilizing the newly developed multi-optical sensing system to monitor the strain and temperature field changes at different welding conditions, and correlate them to the final weld attributes. With additional experimental data, such correlation can be potentially extended to establish a database to monitor and control the welding processes.

Table 2. Feature analysis of measured welding parameters

	Strain at 80 seconds		Temperature peak(° C)		Peak strain	
	5mm	2.5mm	2.5mm	5mm	2.5mm	5mm
I	0.003	0.0013	592	443	0.012	0.01
II	0.0025	0.0013	481	308	0.010	0.008
III	0.00076	-0.0015	435	290	0.0066	0.006

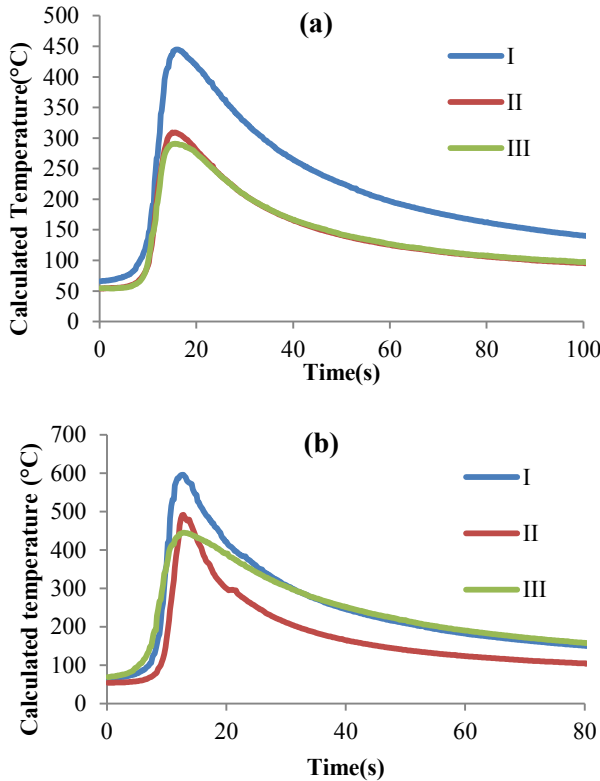


Figure 10 (a) Calculated temperature at 5 mm (b) Calculated temperature at 2.5 mm

In weld experiment IV, the wire feeding position was deliberately misaligned to generate defective weld bead as shown in Fig. 11. The total strain measured at 2.5mm and 5mm away from the fusion boundary of the defective weld is shown in Fig.12. The strain curves are much different from those of good welds in Fig. 9, suggesting the potential to detect weld defects using in-situ DIC strain measurement.

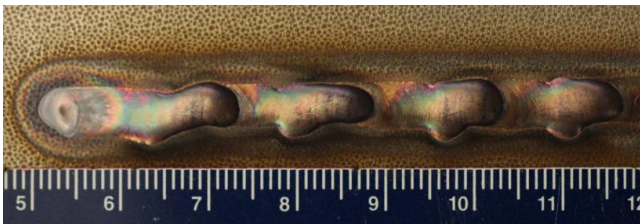


Figure 11 Top view of weld with defect

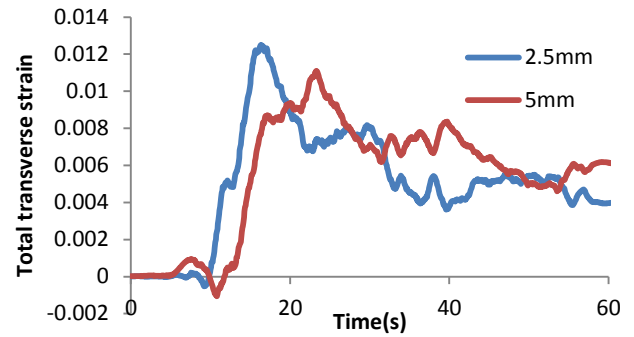


Figure 12 Total transverse strain of weld with defect

IV. CONCLUSION

In this paper, in-situ strain measurement was conducted using DIC and IR multi-sensor system. The strain and temperature adjacent to the weld pool was successfully measured at 2.5 mm close to the edge of the weld. The noise of the DIC full field strain was reduced by filtering.

The experimental data show that changing welding current and speed, as well as the final weld characteristics, can be positively correlated to the variation of measured temperature and strain data. All these effort can provide addition guide to eliminate the potential defect during arc welding.

V. ACKNOWLEDGEMENTS

Research supported by US Department of Energy, Office of Nuclear Energy. This research was sponsored by the US Department of Energy, Office of Nuclear Energy, for Nuclear Energy Enabling Technologies Crosscutting Technology Development Effort, under a prime contract with Oak Ridge National Laboratory (ORNL). ORNL is managed by UT-Battelle, LLC for the U.S. Department of Energy under Contract DE-AC05-00OR22725.

REFERENCES

- [1] S. C. J. Wu, "Software System Designs of Real-time Image Processing of Weld Pool Dynamic Characteristics," in *2006 International Conference on Robotic Welding, Intelligence and Automation*, Shanghai, China, 2006.
- [2] W. Li, Y. Ji, J. Wu, and J. Wang, "A modified welding image feature extraction algorithm for rotating arc narrow gap MAG welding," *Industrial Robot: An International Journal*, vol. 42, pp. 222-227, 2015.
- [3] K. G. W. Li, J. Wu, T. Hu, J. Wang, "SVM-based information fusion for weld deviation extraction and weld groove state identification in rotating arc narrow gap MAG welding," *Int J Adv Manuf Technol*, vol. 74, pp. 1355-1364, 2014.
- [4] S. B. Chen, J. Wu, and Q. Y. Du, "Non-linear modelling and compound intelligent control of pulsed gas tungsten arc welding dynamics," *Proceedings of the Institution of Mechanical Engineers, Part I: Journal of Systems and Control Engineering*, vol. 225, pp. 113-124, February 1, 2011 2011.
- [5] S. Nagarajan, P. Banerjee, W. Chen, and B. A. Chin, "Control of the welding process using infrared sensors," *Robotics and Automation, IEEE Transactions on*, vol. 8, pp. 86-93, 1992.

- [6] I. Eriksson, P. Haglund, J. Powell, M. Sjö Dahl, and A. F. H. Kaplan, "Holographic measurement of thermal distortion during laser spot welding," *Optical Engineering*, vol. 51, pp. 030501-1-030501-3, 2012.
- [7] J. Chen, X. Yu, R. G. Miller, and Z. Feng, "In situ strain and temperature measurement and modelling during arc welding," *Science and Technology of Welding and Joining*, vol. 20, pp. 181-188, 2015/03/18 2015.
- [8] W. Woo, Z. Feng, X. L. Wang, and S. A. David, "Neutron diffraction measurements of residual stresses in friction stir welding: a review," *Science and Technology of Welding and Joining*, vol. 16, pp. 23-32, 2011.
- [9] B. Pan, K. Qian, H. Xie, and A. Asundi, "Two-dimensional digital image correlation for in-plane displacement and strain measurement: a review," *Measurement science and technology*, vol. 20, p. 062001, 2009.
- [10] H. Bruck, S. McNeill, M. A. Sutton, and W. Peters Iii, "Digital image correlation using Newton-Raphson method of partial differential correction," *Experimental Mechanics*, vol. 29, pp. 261-267, 1989.
- [11] B. Pan, A. Asundi, H. Xie, and J. Gao, "Digital image correlation using iterative least squares and pointwise least squares for displacement field and strain field measurements," *Optics and Lasers in Engineering*, vol. 47, pp. 865-874, 2009.
- [12] M. A. Sutton, J. J. Orteu, and H. Schreier, *Image correlation for shape, motion and deformation measurements: basic concepts, theory and applications*: Springer Science & Business Media, 2009.
- [13] B. Pan, H. Xie, Z. Guo, and T. Hua, "Full-field strain measurement using a two-dimensional Savitzky-Golay digital differentiator in digital image correlation," *Optical Engineering*, vol. 46, pp. 033601-033601-10, 2007.
- [14] Y. Zhou, C. Sun, Y. Song, and J. Chen, "Image pre-filtering for measurement error reduction in digital image correlation," *Optics and Lasers in Engineering*, vol. 65, pp. 46-56, 2015.
- [15] B. Pan, "Bias error reduction of digital image correlation using Gaussian pre-filtering," *Optics and Lasers in Engineering*, vol. 51, pp. 1161-1167, 2013.
- [16] H. W. Schreier and M. A. Sutton, "Systematic errors in digital image correlation due to undermatched subset shape functions," *Experimental Mechanics*, vol. 42, pp. 303-310, 2002.
- [17] A. Reynolds and F. Duvall, "Digital image correlation for determination of weld and base metal constitutive behavior," *WELDING JOURNAL-NEW YORK-*, vol. 78, pp. 355-s, 1999.
- [18] C. Leitão, I. Galvão, R. Leal, and D. Rodrigues, "Determination of local constitutive properties of aluminium friction stir welds using digital image correlation," *Materials & Design*, vol. 33, pp. 69-74, 2012.
- [19] B. Grant, H. Stone, P. Withers, and M. Preuss, "High-temperature strain field measurement using digital image correlation," *The Journal of Strain Analysis for Engineering Design*, vol. 44, pp. 263-271, 2009.
- [20] M. De Strycker, P. Lava, W. Van Paepegem, L. Schueremans, and D. Debruyne, "Measuring welding deformations with the digital image correlation technique," *Welding Journal*, vol. 90, pp. 107-112, 2011.
- [21] H. Coules, P. Colegrove, L. Cozzolino, and S. Wen, "Experimental measurement of biaxial thermal stress fields caused by arc welding," *Journal of Materials Processing Technology*, vol. 212, pp. 962-968, 2012.
- [22] W. Cheng, "In-plane shrinkage strains and their effects on welding distortion in thin-wall structures," The Ohio State University, 2005.
- [23] R. Linares, G. Vergara, R. Gutiérrez, C. Fernández, V. Villamayor, L. Gómez, *et al.*, "Laser beam welding quality monitoring system based in high-speed (10 kHz) uncooled MWIR imaging sensors," in *SPIE Sensing Technology+ Applications*, 2015, pp. 948514-948514-7.
- [24] K.-P. Möllmann, F. Pinno, and M. Vollmer, "Two-color or ratio thermal imaging-potentials and limits," 2011.
- [25] T. Nguyen, D. Weckman, D. Johnson, and H. Kerr, "High speed fusion weld bead defects," *Science and Technology of Welding & Joining*, vol. 11, pp. 618-633, 2006.